AUTOPHAGY
2021, VOL. 17, NO. 10, 2749–2765
https://doi.org/10.1080/15548627.2020.1838117

Taylor & Francis
Taylor & Francis Group

RESEARCH PAPER



# PTPN9-mediated dephosphorylation of VTI1B promotes ATG16L1 precursor fusion and autophagosome formation

He-Yen Chou[a], Yi-Tang Lee[a,b*], Yuchieh Jay Lin[a,b,c*], Jung-Kun Wen[a*], Wen-Hsin Peng[a], Pei-Lien Hsieh[a], Shu-Yu Lin[a], Chin-Chun Hung[a], and Guang-Chao Chen [a,b,c]

[a]Institute of Biological Chemistry, Academia Sinica, Taipei, Taiwan; [b]Institute of Biochemical Sciences, College of Life Science, National Taiwan University, Taipei, Taiwan; [c]Chemical Biology and Molecular Biophysics, Taiwan International Graduate Program, Academia Sinica, Taipei, Taiwan

**ABSTRACT**

Macroautophagy/autophagy is an evolutionarily conserved intracellular pathway for the degradation of cytoplasmic materials. Under stress conditions, autophagy is upregulated and double-membrane autophagosomes are formed by the expansion of phagophores. The ATG16L1 precursor fusion contributes to development of phagophore structures and is critical for the biogenesis of autophagosomes. Here, we discovered a novel role of the protein tyrosine phosphatase PTPN9 in the regulation of homotypic ATG16L1 vesicle fusion and early autophagosome formation. Depletion of PTPN9 and its *Drosophila* homolog Ptpmeg2 impaired autophagosome formation and autophagic flux. PTPN9 colocalized with ATG16L1 and was essential for homotypic fusion of ATG16L1$^{+}$ vesicles during starvation-induced autophagy. We further identified the Q-SNARE VTI1B as a substrate target of PTPN9 phosphatase. Like PTPN9, the VTI1B nonphosphorylatable mutant but not the phosphomimetic mutant enhanced SNARE complex assembly and autophagic flux. Our findings highlight the important role of PTPN9 in the regulation of ATG16L1$^{+}$ autophagosome precursor fusion and autophagosome biogenesis through modulation of VTI1B phosphorylation status.

**Abbreviations:** csw: corkscrew; EBSS: Earle's balanced salt solution; ERGIC: ER-Golgi intermediate compartment; ESCRT: endosomal sorting complexes required for transport; mop: myopic; NSF: N-ethylmaleimide-sensitive factor; PAS: phagophore assembly site; PolyQ: polyglutamine; PtdIns3P: phosphatidylinositol-3-phosphate; PTK: protein tyrosine kinase; PTM: posttranslational modification; PTP: protein tyrosine phosphatase; PTPN23/HD-PTP: protein tyrosine phosphatase non-receptor type 23; SNARE: soluble N-ethylmaleimide sensitive factor attachment protein receptor; STX7: syntaxin 7; STX8: syntaxin 8; STX17: syntaxin 17; VAMP3: vesicle associated membrane protein 3; VAMP7: vesicle associated membrane protein 7; VTI1B: vesicle transport through interaction with t-SNAREs 1B; YKT6: YKT6 v-SNARE homolog; ZFYVE1/DFCP1: zinc finger FYVE-type containing 1.

**KEYWORDS**

Autophagosome; ATG16l1; PTPN9; SNARE; VTI1B

## Introduction

Macroautophagy (hereafter autophagy) is an evolutionarily conserved catabolic pathway critical for cell viability and homeostasis. During autophagy, long-lived proteins and organelles are engulfed by double membrane vesicles termed autophagosomes, which subsequently fuse with lysosomes for degradation and recycling [1]. Autophagosome biogenesis is a dynamic and tightly regulated process. Upon induction of autophagy, the ATG machinery is recruited and assembled at one or several phagophore assembly sites (PASs) localized proximal to the ER, and initiates the nucleation of a double-membrane crescent-shaped structure known as the phagophore [2]. The phagophore membrane subsequently expands and encloses its cargos forming the autophagosome. It has been reported that phagophores can be derived from multiple membrane sources, including the ER-Golgi intermediate compartment (ERGIC) and ER-exit sites [3,4], the Golgi apparatus [5], mitochondria [6], the ER-mitochondrial contact sites [7], and the plasma membrane [8]. Moreover, recent studies indicate that recycling endosomes and both ATG9 and ATG16L1 vesicles also contribute to the biogenesis of autophagosomes [9,10,11], though the detailed mechanisms regulating this process remain elusive.

Protein posttranslational modifications (PTMs) have emerged as potent regulators of autophagy [12]. Protein tyrosine phosphorylation by protein tyrosine kinases (PTKs) and protein tyrosine phosphatases (PTPs) is an important cell signaling event involved in the regulation of various cellular processes [13]. Recent studies have implicated tyrosine phosphorylation/dephosphorylation in modulating the autophagy process. It has been reported that EGFR-mediated tyrosine phosphorylation of BECN1 (beclin 1) suppresses autophagy and promotes lung

**CONTACT** Guang-Chao Chen gcchen@gate.sinica.edu.tw Institute of Biological Chemistry, Academia Sinica, Taipei 115, Taiwan
10/08/2020
*These authors contributed equally to this work.
Supplemental data for this article can be accessed here.

cancer progression [14]. Martin et al. showed that loss of PTPRS (protein tyrosine phosphatase receptor type S) increases levels of cellular phosphatidylinositol-3-phosphate (PtdIns3P) and hyperactivates autophagy [15]. However, the molecular mechanisms underlying the role of PTPs in the regulation of autophagosome formation remain largely unknown.

PTPN9/Ptpmeg2 (protein tyrosine phosphatase nonreceptor type 9) contains a unique phosphoinositide-binding Sec14 homology domain at the $NH_2$ terminus [16,17]. In mammals, PTPN9 has been implicated in the regulation of vesicle fusion and transport, as well as playing an important role in various physiological and pathological processes. PTPN9 was reported to promote secretory vesicle fusion through the dephosphorylation of N-ethylmaleimide-sensitive fusion protein NSF [18]. Expression of PTPN9 caused enlarged secretory vesicles and defective cytokine secretion in leukemia cells [19,20]. PTPN9 has also been found to act as a tumor suppressor by inhibiting ERBB2 and EGFR signaling in breast cancer cells [21]. In addition, one recent study has shown that PTPN9 plays an important role in the regulation of insulin signaling in hepatocytes [22]. Silencing of hepatic PTPN9 expression restores insulin sensitivity and improves glycemic regulation in diabetic mice [22], suggesting that PTPN9 inhibition could be a potential therapeutic target for treating type 2 diabetes. In mice, PTPN9 deficiency causes several neurodevelopmental defects and progressive degeneration in glaucoma [20]. Nevertheless, the role of PTPN9 in autophagy has not been elucidated.

In this study, we discovered that the protein tyrosine phosphatase PTPN9/Ptpmeg2 played an important role in the regulation of autophagosome formation in both *Drosophila* and mammals. Ablation of *Drosophila* Ptpmeg2 caused autophagosome formation defects during starvation-induced autophagy and developmental autophagy. In mammalian cells, we found that PTPN9 colocalized with ATG16L1-positive autophagosome precursor vesicles upon starvation-induced autophagy. Knockdown of PTPN9 impaired ATG16L1 precursor homotypic fusion and autophagic flux. Studies in yeast, *Drosophila*, and mammals have indicated the involvement of soluble N-ethylmaleimide-sensitive factor attachment protein receptor (SNARE) proteins in the autophagic process [23]. $ATG16L1^+$ vesicles have been reported to undergo homotypic fusion mediated by the STX7-STX8-VTI1B-VAMP7-containing SNARE complex, and this fusion results in the formation and expansion of phagophores [10]. In this study, we found that PTPN9 interacted with and dephosphorylated VTI1B, promoting SNARE complex assembly, ATG16L1 homotypic fusion, and autophagic flux. Our study further found that *Drosophila* Ptpmeg2 ameliorated polyglutamine (polyQ)-induced toxicity in retina, suggesting that PTPN9/Ptpmeg2 could potentially be targeted therapeutically to modulate autophagy activity in diseases.

## Results

### *PTPN9/Ptpmeg2 regulates autophagosome formation*

To explore the functional role of PTPs in autophagy, we performed genetic analyses to screen for *Drosophila* nonreceptor PTPs that could modulate the formation of autophagosomes. *Drosophila* fat body cells undergo extensive programmed autophagy during late larval stages [24]. Of the PTPs we screened, knockdown of *Ptpmeg2* and *mop* (myopic) with two independent RNAi lines in third-instar larval fat body using the FLP-out GAL4 system dramatically affected the number and size of mCherry-Atg8a-positive puncta, compared to controls (Figure 1A-C and S1A). While ablation of Ptpmeg2 markedly reduced the number of mCherry-Atg8a-positive puncta, mop depletion led to an increase in the number of small mCherry-Atg8a-positive puncta (Figure 1A-C). Mop and its mammalian homolog HD-PTP have been shown to associate with components of the endosomal sorting complex required for transport (ESCRT) complexes which play important roles in the regulation of autophagosome formation [25]. Thus, we decided to focus on the role of Ptpmeg2 in autophagy. We first checked the effect of Ptpmeg2 depletion on starvation-induced autophagy and autophagic flux using the tandem fluorescent-tagged Atg8a (GFP-mCherry-Atg8a) assay [26]. The tandem-tagged Atg8a reporter labels autophagosomes as yellow ($GFP^+$ $mCherry^+$), whereas the GFP fluorescence is rapidly quenched in acidic autolysosomes ($GFP^-$ $mCherry^+$) when autophagosomes and lysosomes are fused. In starved control cells, most of the Atg8a puncta were labeled as $GFP^-$ $mCherry^+$ autolysosomes (Figure 1E-F). In cells expressing RNAi against *Ptpmeg2*, there was a significant reduction of total Atg8a puncta and the ratio of autolysosomes (red, $GFP^-$ $mCherry^+$) to autophagosome (yellow, $GFP^+$ $mCherry^+$), compared to controls (Figure 1D-F), suggesting that depletion of Ptpmeg2 led to the impairment of starvation-induced autophagy. Moreover, we found that overexpression of *Ptpmeg2* in the fed larval fat body dramatically increased Atg8a puncta formation and autophagic flux (Figure S1B-C). Together, these results indicate that Ptpmeg2 promoted autophagosome formation and autophagic flux during nutrient starvation conditions and developmental autophagy.

Next, we investigated whether PTPN9, the mammalian homolog of Ptpmeg2, also played a role in the regulation of autophagy. PTPN9 is endogenously expressed in several cell lines, with the highest expression in neuronal cell lines including Neuro-2a (N2a) and PC12 cells (Figure S2A), and is localized to punctate staining structures (Figure S2B). To determine the role of PTPN9 in the regulation of autophagy, we analyzed LC3 puncta and LC3-II levels in PTPN9 knockdown N2a cells under starvation conditions. As shown in Figure 2A-C and S2C, PTPN9-depleted cells starved with Earle's balanced salt solution (EBSS) with or without the lysosomal inhibitor bafilomycin A1 (BafA1) had striking decreases in LC3 puncta and LC3-II levels. Similarly, ablation of PTPN9 caused a significant decrease of autophagic structures under starvation conditions, compared to controls, as seen under transmission electron microscopy (TEM) (Figure 2D-E). We further examined the effect of PTPN9 overexpression on autophagy. N2a cells were transiently transfected with V5 tagged-*PTPN9* and starved with EBSS. Interestingly, cells expressing *PTPN9* exhibited a marked increase of LC3 puncta

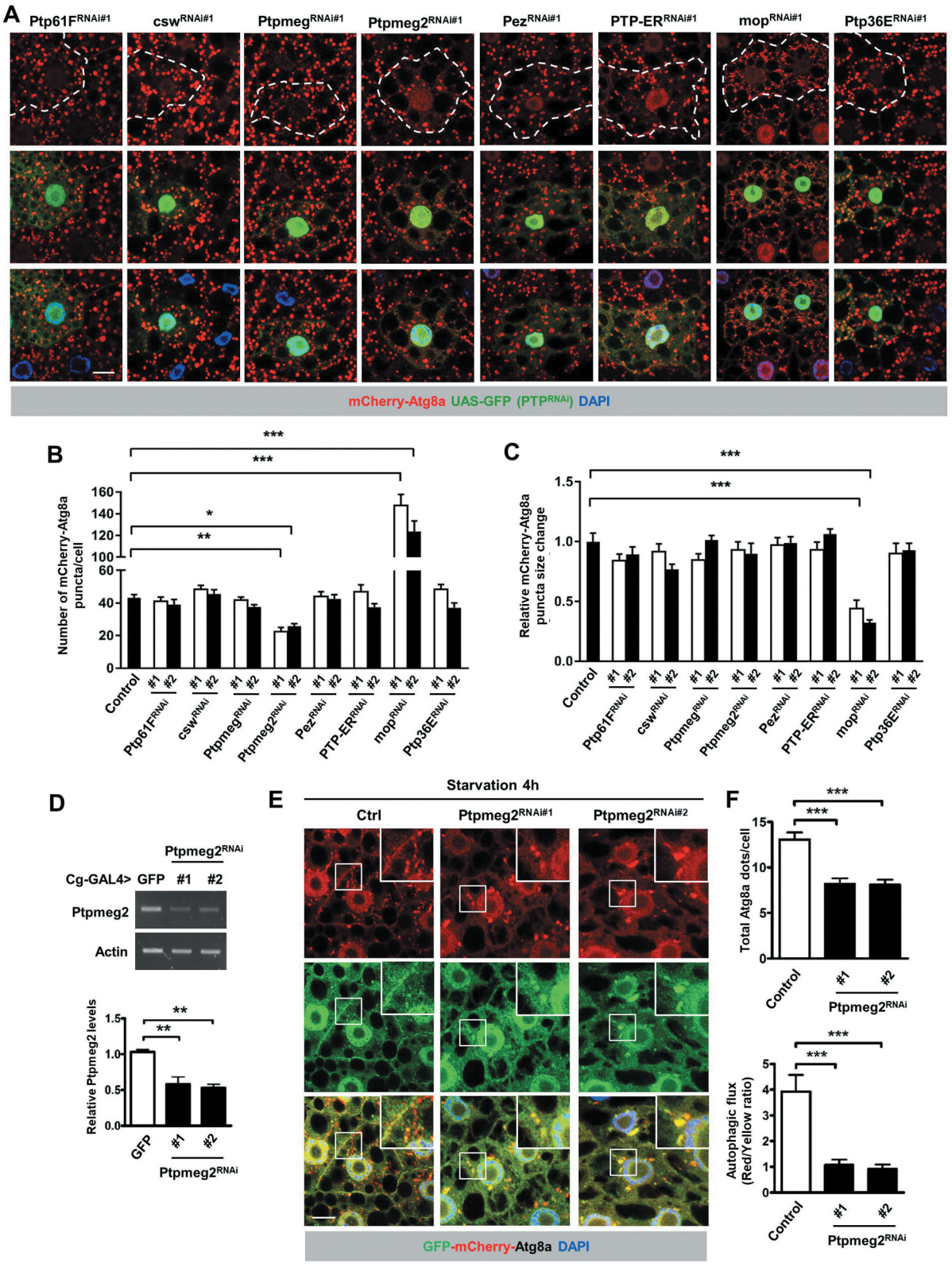


**Figure 1.** Ptpmeg2 depletion impairs developmental and starvation-induced autophagy. (A) RNAi-mediated knockdown of *Drosophila* non-receptor PTPs (GFP-positive clones), including *Ptp61F*, *csw*, *Ptpmeg*, *Ptpmeg2*, *Pez*, *PTP-ER*, *mop*, and *Ptp36E*, in the third instar larval fat bodies using the flp-out system. The mCherry-Atg8a puncta were observed during the developmental autophagic process. Scale bar: 20 μm. (B-C) Quantification of the number (B) and size (C) of mCherry-Atg8a puncta from (A). Data shown as mean ± SEM; n ≥ 10 larvae, ≥ 15 clones per genotype. (D) RT-PCR analysis of *Ptpmeg2* mRNA expression level in control (*Cg-GAL4> GFP*) and Ptpmeg2 knockdown (*Cg-GAL4> Ptpmeg2*$^{RNAi}$) larval fat bodies. The levels of Ptpmeg2 were quantified and expressed as fold changes compared with the control. Data are mean ± SEM of triplicates. (E) Depletion of Ptpmeg2 impairs starvation-induced autophagy. Confocal images of starved early third instar larval fat body of control and *Ptpmeg2*$^{RNAi}$-expressing tandem GFP-mCherry-Atg8a driven by *Cg-GAL4*. (F) Quantification of number of total Atg8a puncta and ratio of acidic autolysosomes (red only) to autophagosomes (yellow) per cell. n ≥ 20 larvae, ≥ 35 cells per genotype. Scale bar: 10 μm. Data shown as mean ± SEM. *P < 0.05; **P < 0.01; *** P < 0.001.

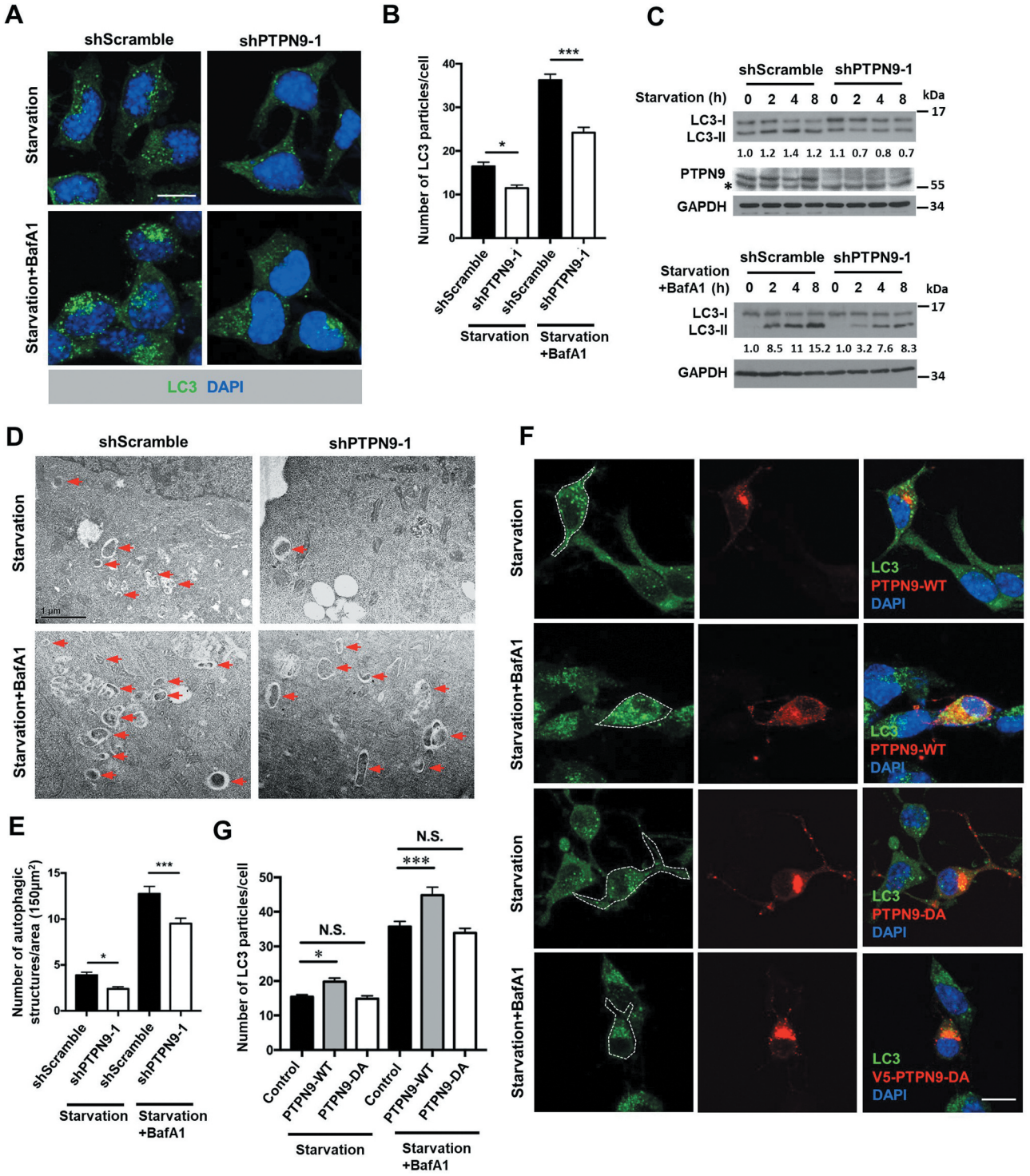


**Figure 2.** PTPN9 acts as a positive regulator of autophagy. (A) N2a cells stable expressing scramble control shRNA or *PTPN9* shRNA were cultured for 2 h in EBSS medium with or without 100 nM lysosomal inhibitor bafilomycin A1 (BafA1) and immunostained with anti-LC3 antibody. Nuclei were stained with DAPI. Scale bar: 10 μm. (B) Quantification of the number of LC3 puncta in control and shPTPN9-1 cells treated as (A); data shown as mean ± SEM, n ≥ 33 cells, *P < 0.05; ***P < 0.001. (C) Cells as in (A) were cultured in EBSS with or without BafA1 for the indicated time points. Effects of PTPN9 knockdown on starvation-induced LC3 conversion were assessed by immunoblotting with antibodies as indicated. Numbers below lanes indicate the relative ratio of LC3-II/GAPDH. Immunoblots were performed at least twice and representative figures are shown. The asterisk indicates nonspecific bands. (D-E) Control and shPTPN9-1 N2a cells were cultured for 2 h in EBSS medium with or without BafA1 and analyzed by transmission electron microscopy (TEM) (D). The autophagic structures (red arrows) were quantified (E). Data shown as mean ± SEM. n ≥ 24 EM micrographs were examined for each sample. *P < 0.05; ***P < 0.001. (F) N2a cells transfected with V5-PTPN9-WT or DA mutant were cultured in EBSS medium for 2 h with or without BafA1. Scale bar: 10 μm. (G) Quantification of the number of LC3 puncta in N2a cells as in (F). Data shown as mean ± SEM; n ≥ 23 cells for each sample; *P < 0.05; ***P < 0.001; NS, not significant.

upon nutrient deprivation in EBSS (Figure 2F), compared with controls. This increase could be due to an increase in autophagosome formation or the blockage of autophagic flux. To determine the possible effects, cells transfected with PTPN9 were treated with BafA1 under starvation conditions. Compared to control cells, BafA1 treatment resulted in significantly increased number of LC3 puncta in PTPN9 expressing cells, suggesting that overexpression of *PTPN9* enhanced the formation of autophagosomes (Figure 2F-G). Moreover, we observed similar numbers of LC3 puncta in controls and cells expressing the PTPN9 catalytically inactive mutant D470A (DA) under starvation conditions (Figure 2F-G), suggesting that the catalytic activity of PTPN9 is essential for its function in regulating autophagy. Taken together, our results demonstrate that PTPN9 plays a positive role in the regulation of autophagosome formation.

### *PTPN9 associates with ATG16L1-positive vesicles*

Diverse membrane sources, including the ER, the Golgi apparatus, mitochondria, recycling endosomes and the plasma membrane, have been found to contribute to the biogenesis of autophagosomes [27]. To determine whether PTPN9 was associated with autophagosomal membrane development during starvation-induced autophagy, we analyzed the colocalization of PTPN9 with a number of autophagosome markers in the autophagic process. These markers included early (ZFYVE1/

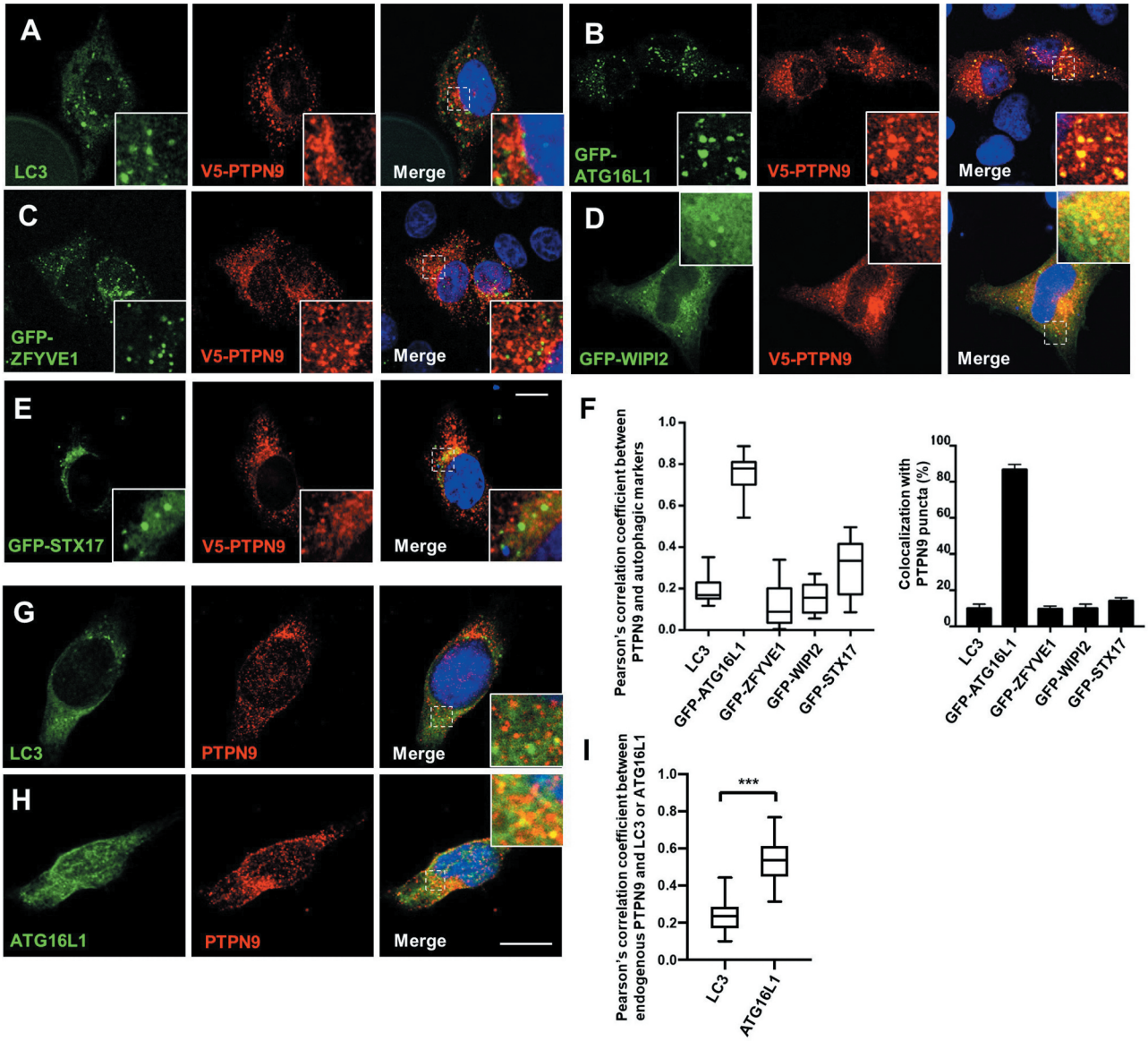


**Figure 3.** PTPN9 is highly colocalized with ATG16L1$^{+}$ vesicles. (A-E) PTPN9 colocalizes with ATG16L1, but not with LC3, ZFYVE1, WIPI2, or STX17. HeLa cells transfected with V5-PTPN9 (red) and an empty vector control (A), GFP-ATG16L1 (B), GFP-ZFYVE1 (C), GFP-WIPI2 (D), or GFP-STX17 (E) were cultured in EBSS for 1 h and immunostained with anti-V5 and/or LC3 antibodies. (F) Quantification of colocalization between PTPN9 and indicated autophagic markers in ≥10 cells as in (A-E). The Pearson's correlation coefficient was analyzed by imageJ. The colocalization percentage was calculated by measuring colocalized pixel map area (yellow puncta) as the numerator and the area of autophagic marker signals as the denominator. (G-H) N2a cells were cultured in EBSS for 2 h and immunostained with anti-PTPN9 and LC3 (G) or ATG16L1 (H) antibodies. (I) Quantification of colocalization between endogenous PTPN9 and LC3 or ATG16L1 in ≥ 24 cells as in (G-H). Data shown as mean ± SEM. ***P < 0.001. Scale bar: 10 μm.

DFCP1, WIPI2, ATG16L1) and later (LC3, STX17) autophagosome markers. It has been previously found that, upon autophagy induction, the double FYVE domain-containing protein ZFYVE1 translocates to PtdIns3P-enriched ER domains called omegasomes [28], and it has been shown that WIPI2 recruits the ATG12–ATG5–ATG16L1 complex to the phagophore for LC3 lipidation and phagophore expansion [29]. Moreover, the autophagic SNARE protein STX17 is known to localize to completed autophagosomes facilitating the fusion between autophagosomes and lysosomes [30]. We found that upon nutrient deprivation, PTPN9 formed the punctate structures in the cytosol and it largely colocalized with GFP-ATG16L1, but not with LC3, GFP-ZFYVE1, GFP-WIPI2, or GFP-STX17 (Figure 3A-F). It has been reported that transiently expressed ATG16L1 affects autophagosome formation and aberrantly targets RAB11$^+$ recycling endosomes [31]. To rule out this possibility, we further checked the colocalization of endogenous PTPN9 and ATG16L1 in N2a cells. As shown in Figure 3G-I, a high percentage of endogenous PTPN9 puncta was also positive for endogenous ATG16L1 but not LC3 under starvation conditions. These findings indicate that PTPN9 plays a role in the early events of autophagosomal membrane formation.

ATG16L1 has been reported to associate with components of clathrin-coated pits and traffics from the plasma membrane to the recycling endosomes and to the sites of autophagosome formation [8]. The endocytic trafficking and homotypic fusion of ATG16L1 precursors are critical to the regulation of autophagosome biogenesis [10]. Therefore, we wanted to explore the colocalization between PTPN9 and endosomes and study the effect of knocking down PTPN9 on ATG16L1$^+$ vesicle trafficking. As shown in Figure S3A-F, the PTPN9 punctate structures colocalized with the recycling endosome markers (GFP-RAB4, GFP-RAB11) and the early endosome marker (GFP-RAB5), but not with the late endosome marker (GFP-RAB7) or the lysosomal marker LAMP1. Moreover, depletion of PTPN9 did not appear to affect either ATG16L1 protein level (Figure S3G) or endocytic trafficking of EGFR (Figure S3H-I), further confirming that PTPN9 played role in ATG16L1-mediated early autophagosome formation.

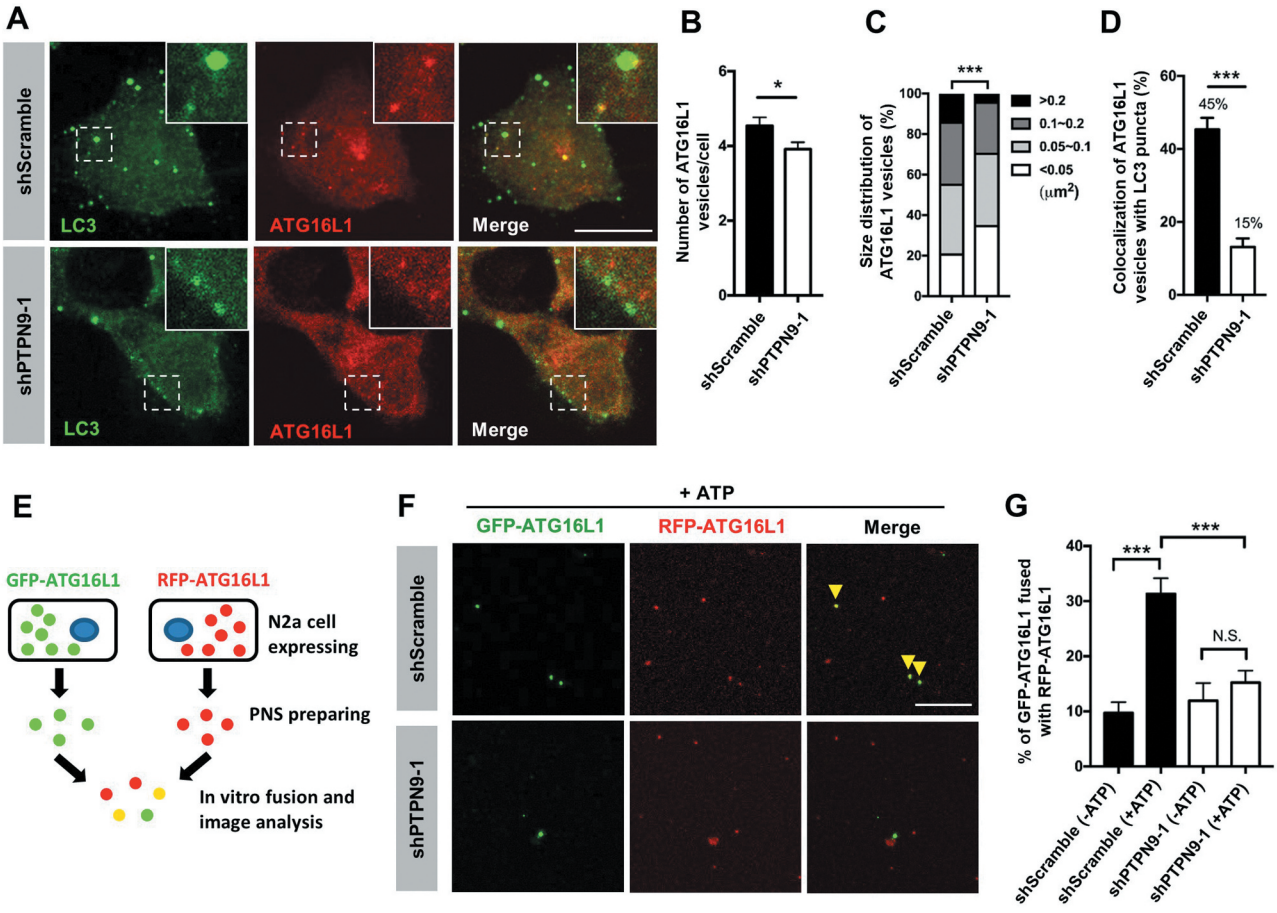


**Figure 4.** PTPN9 regulates homotypic fusion of ATG16L1 vesicles. (A) Control and shPTPN9-1 N2a cells were cultured in EBSS medium for 2 h and immunostained with anti-LC3 (green) and anti-ATG16L1 (red) antibodies. Scale bar: 10 μm. (B-C) Quantification of the number (B) and size (C) of ATG16L1 puncta from (A). Data shown as mean ± SEM; n = 80 for control, n = 110 for shPTPN9 cells. (D) Quantification of colocalization between ATG16L1 and LC3 in control and shPTPN9 N2a cells. Data shown as mean ± SEM; *P < 0.05; ***P < 0.001. (E) Illustration of the *in vitro* membrane fusion assay of ATG16L1 vesicles. (F) Analysis of ATG16L1 vesicles homotypic fusion in vitro. The post-nuclear supernatants (PNS) from control or shPTPN9 N2a cells expressing GFP-ATG16L1 or RFP-ATG16L1 were mixed for the *in vitro* membrane assay in the presence or absence of ATP. Representative confocal images (with ATP) are shown. The fusion vesicles are indicated by arrowheads. (G) Quantification of the homotypic fusion efficiency of ATG16L1 puncta shown in (F). Data shown as mean ± SEM of three experiments. In ATP-treated condition, n = 256 vesicles for control and n = 162 vesicles for PTPN9 shRNA. In ATP-untreated condition, n = 127 vesicles for control and n = 130 vesicles for PTPN9 shRNA. ***P < 0.001; NS, not significant.

### PTPN9 regulates the homotypic fusion of ATG16L1 precursors

Given that the homotypic fusion between ATG16L1 precursors plays a critical role in controlling the size of ATG16L1 vesicles and their maturation into LC3-positive autophagosomes [10], PTPN9 may play a role in regulating ATG16L1 vesicle biogenesis and homotypic fusion. We thus investigated whether PTPN9 knockdown would affect the number and size of endogenous ATG16L1 vesicles under starvation conditions. Immunofluorescence analyses revealed that depletion of PTPN9 in N2a cells markedly decreased endogenous ATG16L1 puncta and the number of large ATG16L1 dots (> 0.2 $\mu m^2$) upon nutrient deprivation, compared with controls (Figure 4A-C). Moreover, the number of ATG16L1 colocalized with LC3 was greatly reduced in PTPN9 knockdown cells (Figure 4D). To confirm that PTPN9 played a role in the regulation of ATG16L1 homotypic fusion, we performed an *in vitro* membrane fusion assay. N2a cells transiently transfected with *GFP-ATG16L1* or *RFP-ATG16L1* were lysed and postnuclear lysates were mixed in the presence or absence of ATP. If the ATG16L1 vesicles underwent homotypic fusion, then GFP-labeled and RFP-labeled ATG16L1 vesicles would merge to generate yellow puncta under fluorescence microscope (Figure 4E). In the presence of ATP, approximately 31% of GFP-ATG16L1 vesicles fused with RFP-ATG16L1 vesicles (Figure 4F-G). Depletion of PTPN9 markedly inhibited the colocalization between GFP-ATG16L1 and RFP-ATG16L1 signals (Figure 4F-G). Considered together, our results indicate that PTPN9 regulates the homotypic fusion of ATG16L1 precursors.

### PTPN9 interacts with SNARE proteins

SNARE-mediated membrane fusion is known to play a pivotal role in various steps of autophagy process including the autophagosome biogenesis and autophagosome-lysosome fusion [23]. Recent studies have indicated that a set of SNARE proteins, including the R-SNARE VAMP7 and the Q-SNAREs STX7 (syntaxin 7), STX8 (syntaxin 8), and VTI1B, are essential for the homotypic fusion of ATG16L1 precursors [10]. We first checked whether PTPN9 might colocalize and interact with these SNARE proteins. Immunofluorescence analysis showed that V5-PTPN9 colocalized with Flag-VTI1B, GFP-VAMP7, GFP-STX7, and STX8 upon nutrient starvation (Figure 5A-D, F). However, PTPN9 has rarely been found to colocalize with GFP-VAMP3 (Figure 5E-F), a reported requirement for fusion of ATG9- and ATG16L1-containing vesicles [32]. Next, we examined whether *PTPN9* knockdown might affect the SNARE complex assembly. Indeed, depletion of PTPN9 markedly reduced VTI1B-VAMP7 interaction and VTI1B-STX8 interaction (Figure 5G-H). The PTPN9-DA mutant, which contains the aspartic acid to alanine mutation in the WPD loop of the PTP domain, has been found to lack catalytic activity but retain its ability to bind target substrates and it has been used as a substrate-trapping mutant [33,34]. We thus checked whether PTPN9-WT and substrate-trapping (DA) mutant could interact with VTI1B, VAMP7, STX7, and STX8 SNARE proteins. Co-immunoprecipitation (Co-IP) analyses showed that Flag-VTI1B, GFP-VAMP7, GFP-STX7, and STX8 interacted with both WT and DA form of PTPN9 (Figure 5I-L). Interestingly, we noticed that GFP-STX7 seemed to be preferentially associated with the PTPN9-DA mutant. These results together suggest that VTI1B, VAMP7, STX7, STX8 might be substrate targets of PTPN9.

### PTPN9 regulates the tyrosine phosphorylation of VTI1B

It has been reported that tyrosine phosphorylation of VAMP7 by Src kinase is important for its function in exocytosis [35]. To test whether VTI1B and STX7 can also be tyrosine phosphorylated, the ectopically expressed VTI1B and STX7 were immunoprecipitated from HEK293T cells with or without the protein tyrosine phosphatase inhibitor pervanadate. An increase of phospho-tyrosine levels was observed in VTI1B and STX7 following pervanadate treatment (Figure 6A and S4A), suggesting that both VTI1B and STX7 can be tyrosine phosphorylated. Notably, we found that only the tyrosine phosphorylation levels of VTI1B, but not VAMP7 or STX7, were dramatically increased in PTPN9 knockdown cells under fed and starvation conditions (Figure 6B and S4B-C). Moreover, VTI1B tyrosine phosphorylation was greatly diminished by co-expression of WT but not the catalytically inactive (CS) form of PTPN9 (Figure 6C). These results suggest that VTI1B could be a bona fide substrate target of PTPN9 during basal and starvation-induced autophagy.

The human VTI1B consists of an N-terminal Habc domain, followed by the C-terminal SNARE motif and a transmembrane domain [36]. Our protein sequence alignments revealed that VTI1B domain structures are conserved across different species, except for *Drosophila* Vti1b which lacks an N-terminal Habc domain (Figure 6D). There are six tyrosine residues in human VTI1B, and bioinformatic analysis indicated that Tyr112 and Tyr115 were likely to be phosphorylated (PhosphoSitePlus Server) (Figure 6D). Indeed, mass spectrometry (MS) analyses of VTI1B purified from controls and PTPN9-knockdown cells identified two unique sites of tyrosine phosphorylation on residues Tyr112 and Tyr115 (Figure S4D-E). We thus mutated tyrosine 112 and 115 of VTI1B to phenylalanine and assayed its tyrosine phosphorylation (pTyr) levels. As shown in Figure 6E, the substitution of Tyr112 or Tyr115 of VTI1B with phenylalanine attenuated the tyrosine phosphorylation of VTI1B in *PTPN9* knockdown cells. Moreover, substitution of both Tyr112 and Tyr115 with phenylalanine (VTI1B-Y2F) almost completely abolished the tyrosine phosphorylation of VTI1B (Figure 6E). These results suggest that PTPN9 may target and dephosphorylate Q-SNARE VTI1B at Tyr112 and Tyr115 residues.

### VTI1B-Y2F mutant promotes ATG16L1 vesicle fusion

VTI1B has been implicated in mediating autophagosome precursor maturation as well as autophagosome-lysosome fusion [10,37]. However, the molecular regulation of VTI1B during autophagy remains unknown. To investigate the functional importance of VTI1B tyrosine phosphorylation on autophagy, we first checked the effects of both phosphomimetic (Y2E)

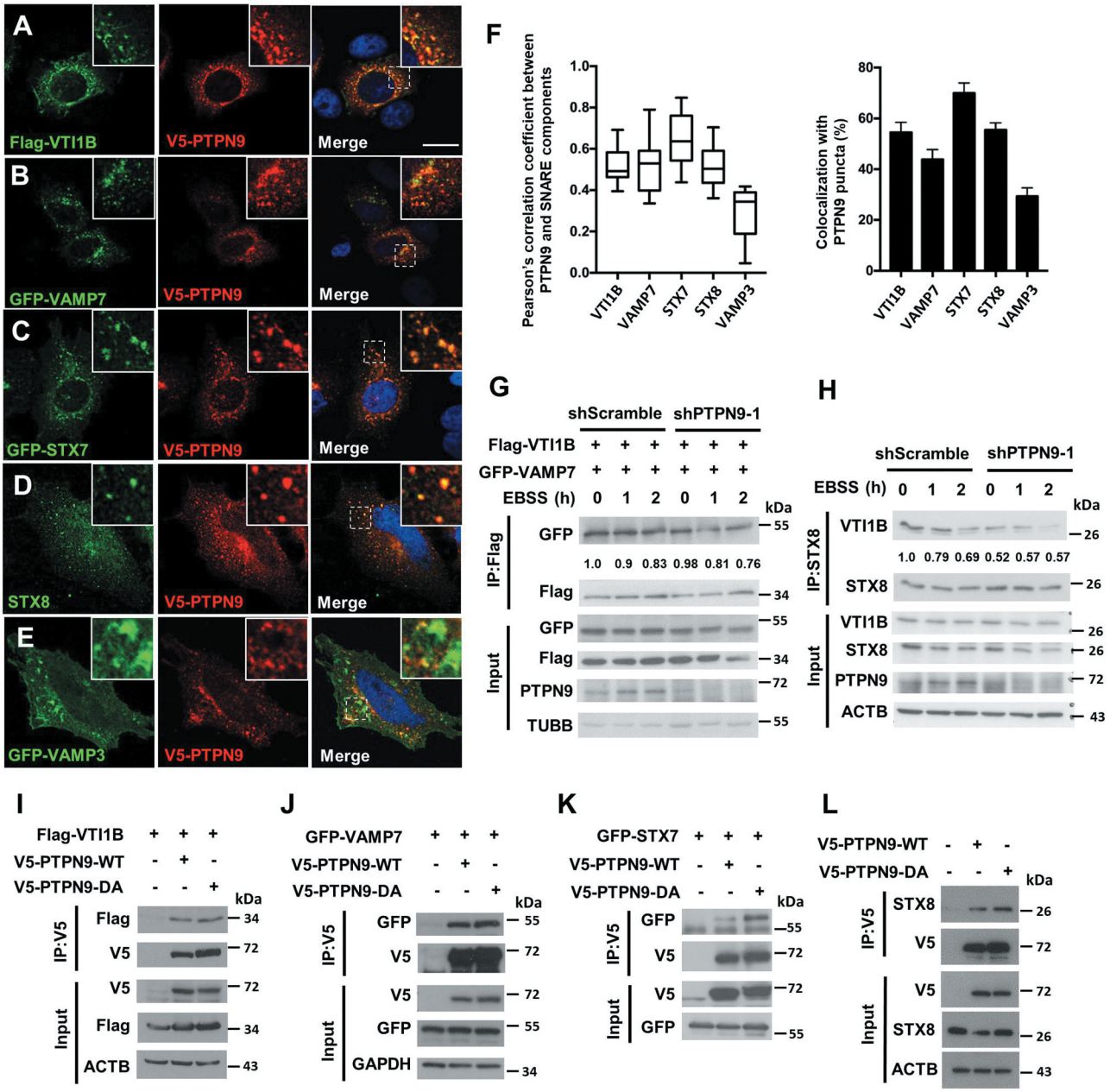


**Figure 5.** PTPN9 interacts and regulates the assembly of STX7/STX8/VTI1B/VAMP7 SNARE complex. (A–E) HeLa cells co-transfected with V5-PTPN9 and Flag-VTI1B (A), GFP-VAMP7 (B), GFP-STX7 (C), GFP-VAMP3 (E), or an empty vector (D) were cultured in EBSS for 1 h and immunostained with indicated antibodies. (F) Colocalization between V5-PTPN9 and the indicated SNARE proteins (yellow puncta) were quantified in ≥ 10 cells as in Figure 3. Scale bar: 10 μm. (G) Ablation of PTPN9 resulted in reduced interaction between VTI1B and VAMP7. Control and shPTPN9 cells transiently transfected Flag-VTI1B and GFP-VAMP7 were cultured in EBSS for the indicated time points and subjected to immunoprecipitations with anti-Flag antibody. The immunoprecipitates and inputs were analyzed by immunoblotting with antibodies as indicated. (H) Ablation of PTPN9 resulted in reduced interaction between VTI1B and STX8. Control and shPTPN9 cells were cultured in EBSS for the indicated time points and subjected to immunoprecipitations with anti-STX8 antibody. The immunoprecipitates and inputs were analyzed by immunoblotting with antibodies as indicated. (I) Co-immunoprecipitation (Co-IP) analysis of interactions between PTPN9 and VTI1B. HEK293T cells transiently transfected with Flag-VTI1B and V5-PTPN9-WT or V5-PTPN9-DA were subjected to immunoprecipitations with anti-V5 antibody. The immunoprecipitates and inputs were analyzed by immunoblotting with antibodies as indicated. (J) Co-IP analysis of interactions between PTPN9 and VAMP7. (K) Co-IP analysis of interactions between PTPN9 and STX7. The experiments in J and K were performed in much the same way as in I. (L) Immunoprecipitation analysis of interactions between PTPN9-WT or DA and endogenous STX8. Immunoblots were performed at least three times and representative figures are shown.

and phosphodefective (Y2F) VTI1B mutants on LC3 puncta formation. N2a cells transiently transfected with Flag-tagged VTI1B-WT, Y2F, or Y2E were starved (EBSS) in the presence or absence or BafA1 and stained with antibodies against LC3 (Figure 7A). Quantitative image analysis showed that, similar to PTPN9, VTI1B-WT and Y2F overexpression increased autophagic flux, whereas VTI1B-Y2E inhibited autophagy (Figure 7A-B). To confirm the role of VTI1B-Y2F in promoting autophagic flux, we further performed the tandem mRFP-GFP-LC3 fluorescence analysis [38]. Cells transfected with *mRFP-EGFP-LC3* and *VTI1B-WT*, *VTI1B-Y2F* or *VTI1B-Y2E* were incubated for 2 h in EBSS. As expected, we found that overexpression of VTI1B-Y2F but not Y2E significantly increased the autolysosome (red, $mRFP^+$ $GFP^-$) to

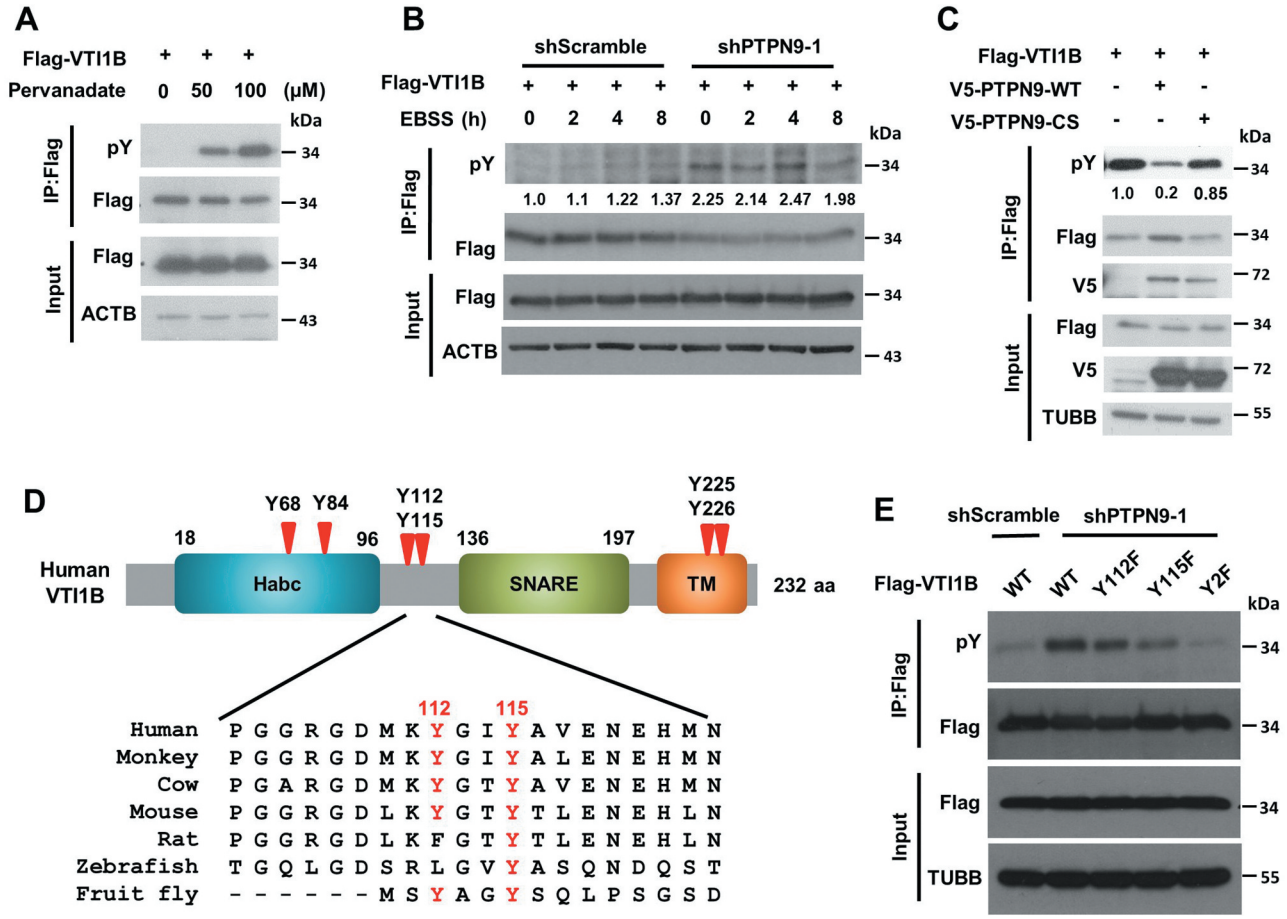


**Figure 6.** VTI1B is a tyrosine-phosphorylated protein and regulated by PTPN9. (A) HEK293T cells transiently transfected with Flag-VTI1B were treated with indicated concentration of pervanadate. Immunoprecipitated VTI1B and cell lysates were subjected to immunoblotting with antibodies as indicated. (B) Ablation of PTPN9 enhanced the tyrosine phosphorylation of VTI1B. Control and shPTPN9 cells transiently transfected with Flag-VTI1B were cultured in EBSS for the indicated time points and subjected to immunoprecipitations with anti-Flag antibody. The immunoprecipitates and inputs were analyzed by immunoblotting with antibodies as indicated. (C) HEK293T cells transiently transfected with Flag-VTI1B and V5-PTPN9-WT or V5-PTPN9-CS were treated with pervanadate, and subjected to immunoprecipitations and immunoblotting analysis. (D) Schematic presentation of the domain structures of human VTI1B (top). An amino acid sequence alignment of the linker region of VTI1B in seven species. The conserved tyrosine residues are marked in red (bottom). (E) Control and shPTPN9 cells transfected with VTI1B WT, Y112 F, Y115F, or Y112 F Y115F (Y2F) mutants were subjected to immunoprecipitation and immunoblotting analysis. Immunoblots were performed at least twice and representative figures are shown.

autophagosome (yellow, $mRFP^+$ $GFP^+$) ratio, compared to controls (Figure S5A-B), suggesting that VTI1B-Y2F plays a positive role in the regulation of starvation-induced autophagy.

Next, we checked whether tyrosine phosphorylation of VTI1B might regulate its localization to $ATG16L1^+$ vesicles upon activation of autophagy. Intriguingly, we found high levels of colocalization between VTI1B-WT or Y2F mutant and $ATG16L1^+$ vesicles under starvation conditions (Figure S5C-D), while VTI1B-Y2E phosphomimetic mutant rarely colocalized with $ATG16L1^+$ vesicles (Figure S5C-D). We further examined the effects of VTI1B mutants in the biogenesis and fusion of ATG16L1 vesicles in VTI1B knockdown cells. Confocal immunofluorescence analysis of endogenous ATG16L1 showed that ablation of VTI1B in starved N2a cells caused a significant decrease in the size of $ATG16L1^+$ vesicles, compared to controls (Figure 7C, E). However, in contrast with previous report [10], the number of $ATG16L1^+$ vesicles did not appear to be affected in VTI1B depleted N2a cells (Figure 7C-D). Re-expression of VTI1B-WT or Y2F but not Y2E dramatically increased the number and size of $ATG16L1^+$ vesicles in VTI1B knockdown cells (Figure 7C-E), indicating that VTI1B dephosphorylation positively regulated the biogenesis and fusion of ATG16L1 vesicles under starvation conditions. This finding is consistent with our observation that VTI1B-Y2F enhanced the formation of the VAMP7-STX8-VTI1B trans-SNARE complex (Figure S5E). Importantly, we found that the decreased number and size of $ATG16L1^+$ vesicles of *PTPN9* knockdown cells could be significantly restored by VTI1B-Y2F overexpression (Figure 7F-H), further confirming that VTI1B acts as a downstream target of PTPN9.

It has been reported that PTPN9 promotes membrane fusion by dephosphorylating the AAA ATPase N-ethylmaleimide-Sensitive Factor (NSF) at Tyr83 [18]. NSF plays an essential role in regulating SNARE complex disassembly and membrane fusion. Recently, Abada et al. showed that inhibition of NSF disturbed the fusion of autophagosome and lysosome [39], yet its function in autophagosome biogenesis has not been directly addressed. To determine the importance of NSF tyrosine phosphorylation in autophagosome biogenesis, we examined the effects of NSF dominant negative mutant (E329Q) and NSF phosphodefective mutant (Y83F) on ATG16L1 vesicle

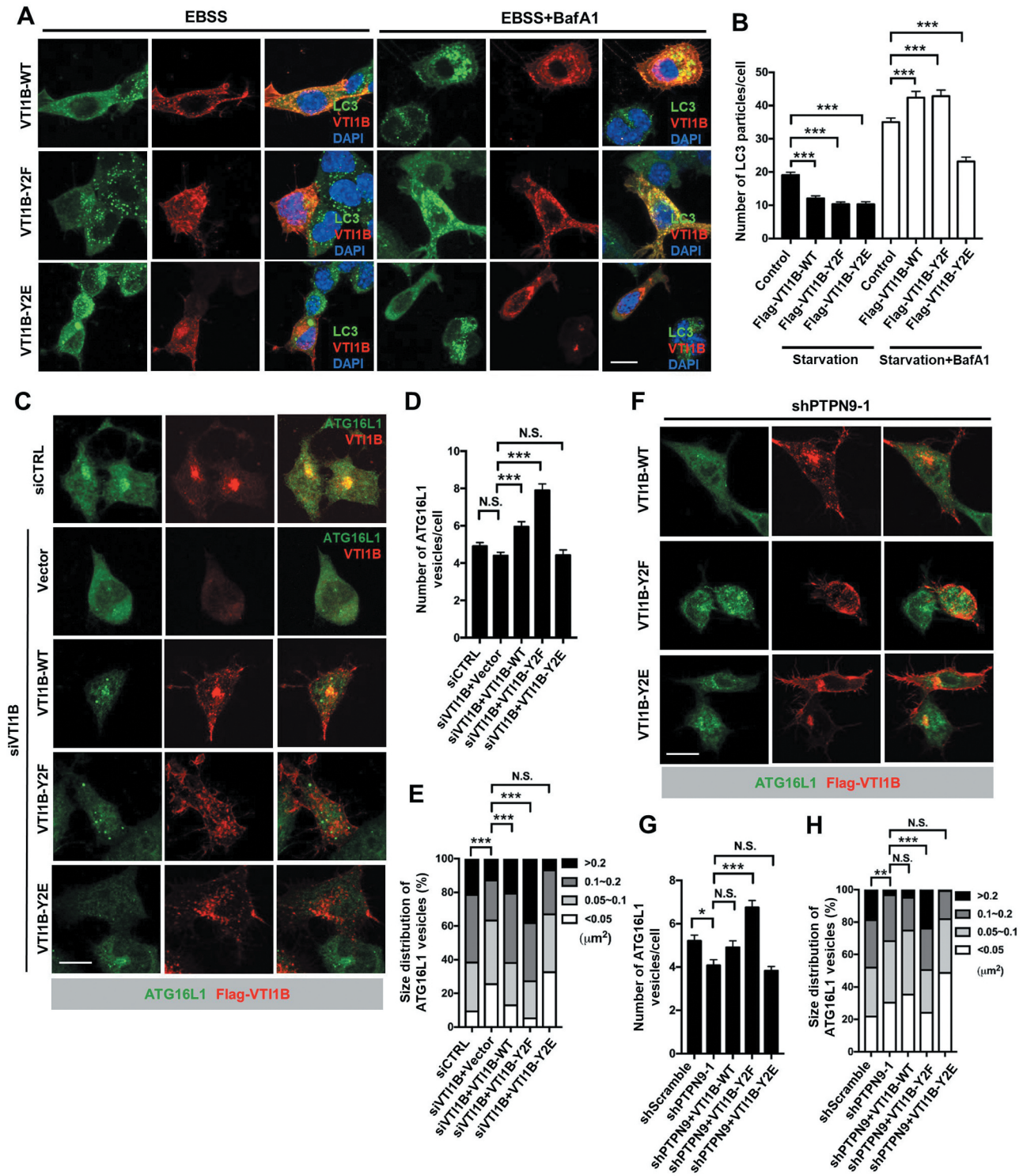


**Figure 7.** The VTI1B tyrosine phosphorylation-defective mutant (VTI1B-Y2F) promotes fusion of ATG16L1 vesicles and autophagic flux. (A) N2a cells transiently transfected with Flag tagged VTI1B-WT, Y2F or Y2E were cultured for 2 h in EBSS medium with or without 100 nM BafA1 and immunostained with anti-LC3 and anti-Flag antibodies. Scale bar: 10 μm. (B) Quantification of the number of LC3 puncta per cell in (A). Nuclei were stained with DAPI. Data shown as mean ± SEM; n ≥ 23 cells for each; ***P < 0.001. (C) Control (siCTRL) and siVTI1B N2a cells transfected with empty vector control or siRNA resistant Flag-VTI1B-WT, Y2F, or Y2E were cultured in EBSS for 2 h and immunostained with anti-Flag and anti-ATG16L1 antibodies. Scale bar: 10 μm. (D-E) Quantification of the number (D) and size (E) of ATG16L1 puncta in cells from (C). Data shown as mean ± SEM; n ≥ 49 cells for each; **P < 0.01; ***P < 0.001; NS, not significant. (F) shPTPN9 N2a cells transfected with Flag-VTI1B-WT, Y2F, or Y2E were cultured in EBSS for 2 h and immunostained with anti-Flag and anti-ATG16L1 antibodies. Scale bar: 10 μm. (G-H) Quantification of the number (G) and size (H) of ATG16L1 puncta in cells from (F). Data shown as mean ± SEM; n ≥ 38 cells for each; **P < 0.01; ***P < 0.001; NS, not significant.

biogenesis and membrane fusion under starvation conditions. While the dominant negative NSF-E329Q mutant caused a decrease in the population of the large-sized ATG16L1$^+$ vesicles, the phosphodefective NSF-Y83F mutant did not affect the number or size of ATG16L1$^+$ vesicles, compared to controls (Figure S5F-G). Together, these results indicate that PTPN9-

mediated dephosphorylation of VTI1B plays an important role in regulating ATG16L1$^{+}$ vesicle fusion and autophagosome formation.

### *Overexpression of Drosophila Ptpmeg2 attenuates the polyglutamine toxicity*

Autophagy dysregulation has been shown to associate with several human neurodegenerative disorders, including polyglutamine (polyQ) diseases [40,41]. Since PTPN9 promotes ATG16L1 homotypic fusion and autophagy induction, possibly conferring some neuroprotection during neurodegeneration, we tested whether modulating levels of Ptpmeg2 could mitigate the polyglutamine toxicity in *Drosophila*. It has been reported that ectopic expression of glutamine repeats in *Drosophila* developing eyes results in accumulation of ubiquitinated protein aggregates and eye degeneration [42]. Indeed, ectopic expression of polyQ proteins containing the expanded 41 glutamine repeats (41Q) in developing eyes with the *GMR-GAL4* driver caused a dramatic increase in the number of ubiquitin-positive aggregates, whereas co-expression of Ptpmeg2 attenuated this staining pattern (Figure 8A). The adult *Drosophila* compound eye consists of approximately 800 hexagonal unit eyes known as ommatidia [43]. In a given section plane, the wild-type control adult fly eyes were observed to have a highly precise array of seven photoreceptor neurons in each ommatidium (Figure 8B). However, expression of 41Q in adult fly eyes caused an age-dependent disruption of the regular array of ommatidia and loss of intact rhabdomeres (Figure 8C, F-G). Notably, co-expression of Ptpmeg2 significantly rescued the 41Q-induced degeneration defects, since most of the ommatidia displayed the characteristic seven rhabdomeres in a near normal pattern in one-day-old adult flies ($P < 0.001$) (Figure 8D, F). This rescue was also observed at days 3 ($P < 0.001$) and 5 ($P < 0.05$) (Figure 8D, F). In contrast, depletion of Ptpmeg2 exacerbated the degeneration defects with markedly reduced number of intact rhabdomeres in the ommatidia (Figure 8E, F). Thus, our in vivo analyses in *Drosophila* indicated that Ptpmeg2 overexpression ameliorated the polyglutamine toxicity.

## Discussion

In this study, we revealed a novel role of the nonreceptor tyrosine phosphatase PTPN9/Ptpmeg2 in the regulation of early autophagosome formation. While PTPN9 overexpression accelerated autophagic flux, depletion of PTPN9 impaired autophagosome formation by reducing the homotypic fusion of ATG16L1 precursors. It has been previously shown that trafficking and homotypic fusion of ATG16L1 precursors play important roles in autophagosome biogenesis [10]. In addition, the SNARE proteins, including the R-SNARE VAMP7 and the Q-SNAREs STX7 (syntaxin 7), STX8 (syntaxin 8), and VTI1B, have been implicated in the regulation of the homotypic fusion of ATG16L1 precursors for autophagosome biogenesis [10]. Interestingly, we found that PTPN9 interacts with and dephosphorylates tyrosine-phosphorylated SNARE protein VTI1B. Like PTPN9, overexpression of the phospho-deficient VTI1B mutant increases ATG16L1 precursor fusion and autophagic flux. These findings identify PTPN9 as a novel regulator of autophagosome biogenesis (Figure 8H).

SNARE-mediated membrane fusion has been shown to regulate early autophagosome biogenesis and autophagosome maturation. In the early phase of autophagosome formation, the SNARE proteins including VTI1B, STX7, STX8, VAMP7, and VAMP3 have been shown to regulate the homotypic fusion of ATG16L1-positive vesicles and the heterotypic fusion between ATG16L1- and ATG9-containing vesicles [10,32], which subsequently contributes to the expansion of phagophores and autophagosome formation. In the process of autophagosome maturation, the SNAREs, including STX17, VAMP8, SNAP29, YKT6, and STX7, have been found to mediate autophagosome–lysosome fusion [44]. However, the molecular regulation of SNAREs in autophagy remains largely unclear. One of the strategies to regulate SNAREs is by post-translational regulation. In fact, it has been reported that O-GlcNAcylation of the SNAP29 regulates autophagosome maturation [45]. Moreover, phosphorylation also appears to act as a regulatory mechanism for controlling the function of SNAREs during membrane trafficking and fusion. Several recent studies have shown that phosphorylation of SNAREs and their regulators causes conformational changes and modulates their biological activity. For instance, Malmersjo et al. found that serine/threonine phosphorylation of the SNARE domain of VAMP8 prevented vesicle fusion and suppressed cell secretion [46]. Burgo et al. showed that tyrosine phosphorylation of the longin domain of VAMP7 enhanced its interaction with t-SNAREs and promotes axonal growth and exocytosis in neurons [35]. Phosphorylation has also been found in the SNAP family including SNAP25, SNAP23, and SNAP29 [47]. Despite these findings, the involvement of SNARE phosphorylation in autophagy remains unclear.

Here we found that PTPN9 plays an important role in the regulation of the assembly of SNAREs involved in ATG16L1 homotypic fusion. Co-IP assays showed that both the WT and DA forms of PTPN9 interacted with VTI1B, VAMP7, STX7, and STX8, raising the possibility that these SNARE proteins might be substrate targets of PTPN9. However, we found that only the tyrosine phosphorylation levels of VTI1B, but not VAMP7 or STX7, were dramatically increased in PTPN9 knockdown cells under fed and starvation conditions, suggesting that VTI1B could be a bona fide substrate target of PTPN9 during basal and starvation-induced autophagy. We further showed that PTPN9 modulated the phosphorylation of VTI1B at Y112 and Y115. Like other VTI1 family proteins, VTI1B contains an N-terminal Habc domain, a SNARE motif, and a C-terminal transmembrane domain [36]. Structural analyses showed that Y112 and Y115 are located at the linker region between the Habc domain and SNARE motif of VTI1B. Thus, tyrosine phosphorylation/dephosphorylation of VTI1B at Y112 and Y115 may play a regulatory role in VTI1B conformation and function. Indeed, like PTPN9, ectopic expression of VTI1B tyrosine phosphorylation deficient mutant VTI1B-Y2F (Y112F Y115F) enhanced SNARE complex formation, ATG16L1-positve vesicles and autophagic flux. Moreover, we found that, unlike the VTI1B-WT and Y2F mutant, the phosphomimetic VTI1B-Y2E mutant does not colocalize with ATG16L1$^{+}$ vesicles. Interestingly, Kumar et al. recently showed that phosphorylation of STX17 by TBK1 translocates STX17 to phagophore assembly sites to

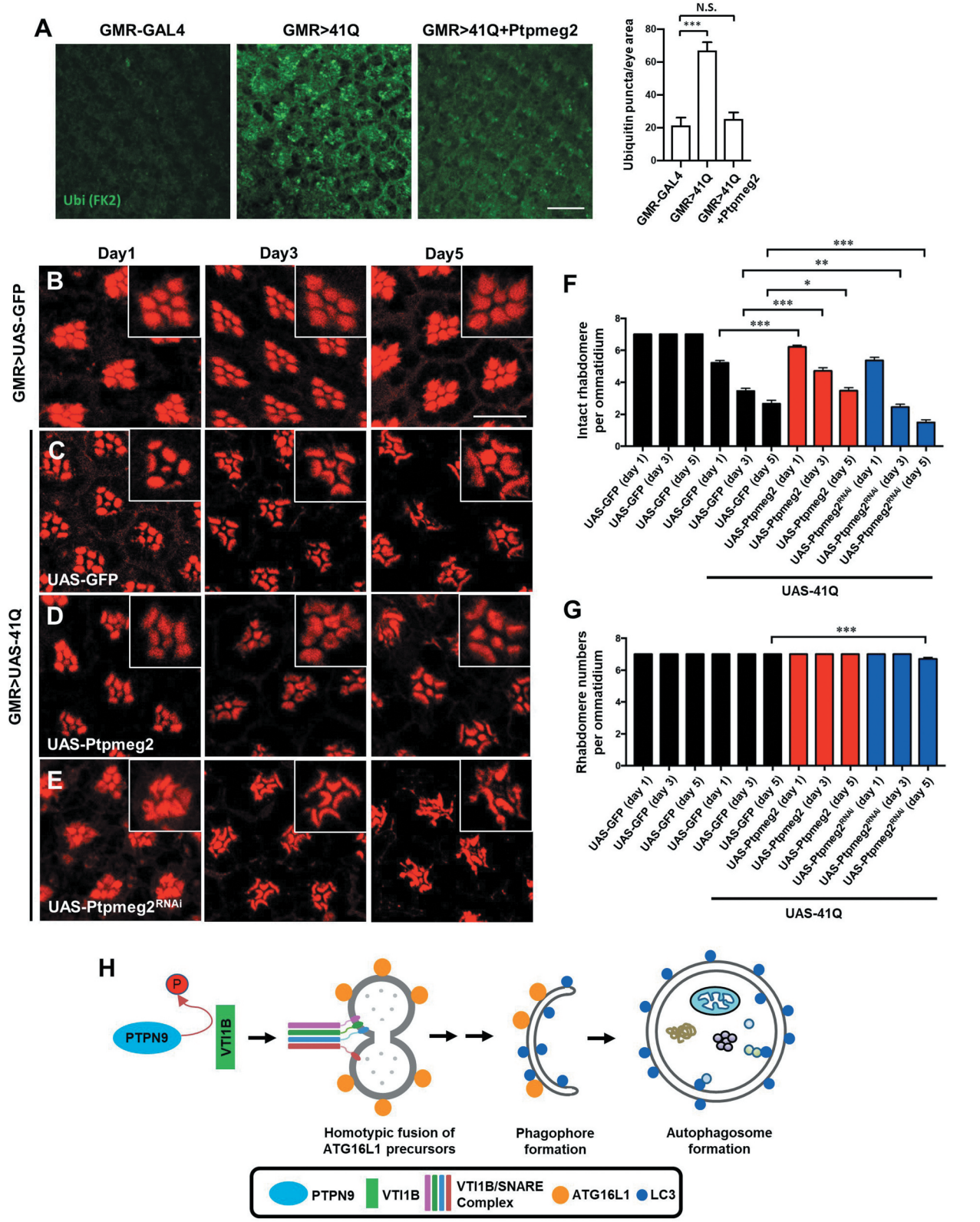


**Figure 8.** Ptpmeg2 overexpression attenuates the polyglutamine toxicity in the fly retina. (A) Overexpression of Ptpmeg2 in developing eyes attenuates polyglutamine (41Q) induced ubiquitinated protein aggregates. Confocal images of third-instar larval eye imaginal discs from *GMR-GAL4* controls or flies expressing indicated transgenes stained with anti-ubiquitin (FK2) antibody. The number of ubiquitin-positive aggregates was quantified. Data shown as mean ± SEM; n ≥ 17 for each genotype; ***P < 0.001. Scale bar: 10 μm. (B-E) Confocal images of phalloidin stained retinae from 1-, 3-, and 5-day old adult flies expressing GFP (control) alone or 41Q together with GFP, Ptpmeg2, or Ptpmeg2$^{RNAi}$ under control of the eye-specific driver *GMR-GAL4*. Scale bar: 10 μm. (F-G) Quantification of intact (F) and total (G) rhabdomere numbers in flies described in (A-D). Thirty ommatidia from ten animals were examined for each genotype. Data shown as mean ± SEM; *P < 0.05; **P < 0.01; ***P < 0.001. (H) Schematic model showing that PTPN9 promotes SNARE complex assembly and autophagosome precursor maturation through the dephosphorylation of the SNARE protein VTI1B.

regulate ULK1 complex assembly and autophagy initiation [48]. Our findings thus revealed a new role of SNARE phosphorylation in the regulation of autophagy.

VTI1B is a highly conserved Qb SNARE protein that has been reported to regulate endolysosomal trafficking, retrograde transport and synaptic vesicle secretion [36]. Recently, together with VAMP3-STX6 and VAMP8, VTI1B has also been implicated in regulating recycling endosome-autophagosome and autophagosome-lysosome fusion [37,49]. Our findings revealed that PTPN9 and VTI1B dephosphorylation played an important role in the regulation of ATG16L1-mediated early autophagic events. We found that, upon nutrient starvation, PTPN9 was highly colocalized with ATG16L1$^+$ vesicles but not with the autophagosome marker LC3, the late endosome marker RAB7, or the lysosome marker LAMP1, suggesting a specific role of PTPN9 in regulating the early steps of autophagosome formation. Besides VTI1B, the SNARE priming enzyme NSF is also known to be a substrate target of PTPN9 [18]. Interestingly, Abada et al. showed that SNARE priming was essential for autophagosome maturation but not for autophagosome biogenesis [39]. Consistent with their findings, our results showed that expression of the phospho-deficient (Y83F) mutant form of NSF did not affect the number or size of ATG16L1 puncta. Moreover, several lines of evidence indicate that PTPN9-mediated VTI1B dephosphorylation regulates ATG16L1 vesicle biogenesis and homotypic fusion. First, immunofluorescence analysis showed that depletion of PTPN9 or VTI1B in N2a cells markedly reduced the number and size of ATG16L1 puncta upon nutrient deprivation. It is interesting to note that our results are different from a previous study which observed an increase of small ATG16L1 vesicles in VTI1B depleted cells [10]. The difference between our findings and the previous observations could be due to differences in cell types used or limitations (antibody sensitivity) in analytical technique. Second, we found that re-expression of VTI1B-Y2F but not Y2E in VTI1B knockdown cells significantly increased the number and size of endogenous ATG16L1$^+$ vesicles. Third, we showed that overexpression of VTI1B-Y2F significantly increased the number and size of ATG16L1$^+$ vesicles in PTPN9 knockdown cells. These results together strongly indicate the importance of PTPN9-mediated VTI1B dephosphorylation in the regulation of the biogenesis and fusion of ATG16L1 vesicles under starvation conditions.

The ubiquitin–proteasome system and autophagy are two major pathways responsible for the degradation of misfolded proteins [50]. Impaired autophagy leads to accumulation of protein aggregates, contributing to neurodegeneration [40]. Polyglutamine disorders are caused by the expansion of CAG repeats within the coding region of affected genes, and they are characterized by the accumulation of protein aggregates that result in neuronal dysfunction and death [41,51]. Consistent with our findings on the role of PTPN9/Ptpmeg2 in regulating autophagy, we also found that Ptpmeg2 could act as a modifier of polyglutamine-associated neurodegeneration in vivo using a *Drosophila* model. The validation of PTPN9 function in mammalian polyglutamine disease model will be the subject of future studies.

## Materials and methods

### Drosophila strains and genetics

Unless noted, all flies were raised at 25°C following standard procedures. The fly strains used in this study were as follows: *GMR-GAL4*, *Cg-GAL4*, *UAS-GFP*, *UASp-mCherry-GFP-Atg8a* (BL37749) and *UAS-Ptp61F*$^{RNAi\#1}$ (BL32426), *UAS-mop*$^{RNAi\#1}$ (BL32916), *UAS-PTP-ER*$^{RNAi\#1}$ (BL32359), *UAS-Ptpmeg2*$^{RNAi\#2}$ (BL57009), *UAS-csw*$^{RNAi\#2}$ (BL33619), *UAS-Ptpmeg*$^{RNAi\#2}$ (BL39007), *UAS-Pez*$^{RNAi\#2}$ (BL33918), and *UAS-Ptp36E*$^{RNAi\#2}$ (BL65919), which were obtained from the Bloomington Stock Center; *UAS-Ptpmeg2*$^{RNAi\#1}$ (v104427), *UAS-csw*$^{RNAi\#1}$ (v108352), *UAS-Pez*$^{RNAi\#1}$ (v108301), *Ptp36E*$^{RNAi\#2}$ (v102397) obtained from the Vienna *Drosophila* Resource Center (VDRC); *UAS-Ptpmeg*$^{RNAi\#1}$, *UAS-Ptp61F*$^{RNAi\#2}$, *UAS-PTP-ER*$^{RNAi\#2}$ and *UAS-mop*$^{RNAi\#2}$ described previously [52]; and *UAS-41Q*, which was a gift from Horng-Dar Wang [53]. *UAS-Flag-Ptpmeg2* was generated by subcloning *Ptpmeg2* from LD27988 (*Drosophila* Genomics Resource Center (DGRC)) into the pUAST vector (DGRC). The GFP-marked clones in larval fat body were generated using the FLP-out technique as described previously [54]. To induce autophagy in *Drosophila* larval fat bodies, 2$^{nd}$ instar larvae were fed high-nutrient food for 16 h and then starved in 20% sucrose for 4 h. For developmental autophagy, third-instar larvae (96 h after hatching at 25°C) raised on normal food were collected for experiments.

### Cell culture, transfection, and drug treatment

HeLa, HEK293T, MCF7 (gifts from Ruey-Hwa Chen, Academia Sinica), U2OS (BCRC, 60187), and mouse neuroblastoma Neuro-2a (N2a) cells (gifts from Yi-Shuian Huang, Academia Sinica) were cultured at 37°C in Dulbecco's modified Eagle's medium (DMEM; Gibco, 12860–017) supplied with 10% fetal bovine serum (FBS) and 1% antibiotic (penicillin-streptomycin). PC12 cells (gifts from Ruey-Hwa Chen, Academia Sinica) were cultured at 37°C in RPMI-1640 medium supplied with 10% horse serum and 5% FBS. To induce autophagy, cells were washed with PBS (Gibco, 70011–044) and incubated in Earle's balanced salts solution (EBSS; Sigma, E3024-50024) for the indicated times with or without 100 nM bafilomycin A1 (Calbiochem, 196000). Plasmids were transfected into cells using PolyJet transfection reagent (SignaGen).

### Plasmids and siRNAs

The V5-PTPN9 was generated by subcloning *PTPN9* from BC071574 (TransOmic, clone ID: BC071574) into pcDNA3.1 (Invitrogen, V790-20). The V5-PTPN9 DA (D470A) and CS (C515S) mutants were generated by site-direct mutagenesis. The GFP-STX17 plasmid was generated by subcloning *STX17* from Flag-STX17 (Addgene, 45911; deposited by Noboru Mizushima) into pEGFP-C3 (Clontech, 6082–1). pEGFP-ATG16L1, RFP-ATG16L1 and GFP-mATG9 were kindly provided by Wei-Yuan Yang (Academia Sinica). pEGFP-ZFYVE1/DFCP1 was a kind gift from Nicholas Ktistakis (Babraham Institute). The GFP-WIPI2 plasmid was obtained from Ruey-Hwa Chen (Academia Sinica).

GFP-VAMP3 was a gift from Ichiro Nakagawa (Kyoto University). GFP-tagged RAB4, RAB5, RAB7, and RAB11 were obtained as previously described [52]. Flag-VTI1B (45914; deposited by Noboru Mizushima), pEGFP-VAMP7 (42316; deposited by Thierry Galli), GFP-STX7 (45921; deposited by Noboru Mizushima), and mRFP-EGFP-LC3 (21074; deposited by Tamotsu Yoshimori) were acquired from Addgene. Flag-VTI1B Y2F (Y112 F, Y115F) and Y2E (Y112E, Y115E) mutants were generated by site-direct mutagenesis. The Flag-NSF was generated by subcloning *NSF* from BC030613 (TransOmic, clone ID: BC030613) into pcDNA3.1. Flag-NSF-Y83F were generated by site-direct mutagenesis. Myc-NSF-E329Q was a kind gift from Zvulun Elazar (Weizmann Institute of Science). The lentiviral shRNA clones used to knockdown *PTPN9* were obtained from the National RNAi Core Facility of Academia Sinica. The sequences of *PTPN9* shRNAs are shPTPN9-1, 5′-GAGUGCCAAGCACGUUUAUAA-3′ (corresponding to *PTPN9* mRNA: 2776 ~ 2796), and shPTPN9-2, 5′-CCUUUCCCUUUGGCUAGAUAA-3′ (corresponding to *PTPN9* mRNA: 2467 ~ 2487). Sequences of siRNA targeting against *VTI1B* mRNA 3′UTR are siVTI1B, 5′-CCUUGUGGACCAGCAUCUUTT-3′.

### Antibodies

Antibodies used for this study were anti-PTPN9 (R&D system, MAB2668), anti-LC3 (Cell Signaling Technology, 4108), anti-LC3 (Novus, NB100-2220), anti-LC3 (MBL, M152-3), anti-ATG16L1 (MBL, PM040), anti-LAMP1 (Cell Signaling Technology, 9091), anti-EGFR (Cell Signaling Technology, 4267), anti-Flag M2 (Sigma, F1804), anti-VTI1B (BD, 611405), anti-V5 (Bio-Rad, MCA1360), anti-MYC (Santa Cruz Biotechnology, SC-40), anti-HA (Sigma, H9658), anti-GAPDH (Cell Signaling Technology, 5174), anti-ACTB/β-actin (Novus, NB600-501), anti-TUBB/beta-tubulin (Sigma, T0198), anti-GFP (Abcam, ab290), anti-STX8 (BD, 611352), anti-ubiquitin (FK2; Sigma, ST1200) and anti-phospho tyrosine (Merck Millipore, 05–321).

### Immunoprecipitation and western blotting

For immunoprecipitation, cells were lysed in IP lysis buffer (50 mM Tris–HCl, pH 7.4, 150 mM NaCl, 1 mM EDTA, 1% NP-40 [Sigma, 13021], 5 mM NaF, 2 mM $Na_3VO_4$) with protease inhibitor cocktail (Roche, 4693132001) for 40 min on ice. Cell lysates were immunoprecipitated with the indicated antibodies overnight at 4°C with rocking, followed by protein G-Sepharose beads (GE Healthcare, 17061802) affinity isolation at 4°C for 2 h. Beads were washed three times with the IP lysis buffer and eluted with 2x SDS sample buffer at 95°C for 10 min. Proteins were separated by SDS-polyacrylamide gel electrophoresis (SDS-PAGE) and blotted onto PVDF membranes (Millipore, IPVH00010). Membranes were blocked in 5% nonfat dry milk in PBS with 0.1% Tween-20 (Sigma, P1379) for 1 h at room temperature, followed by incubation in indicated primary antibodies overnight at 4°C, washing, and then incubation in secondary HRP-conjugated antibodies for 2 h at room temperature. The western blots were detected with ECL reagent (Millipore, WBKLS0500). For quantification, densitometric analysis was performed using ImageJ software (NIH).

### Immunofluorescence

*Drosophila* larval fat bodies and adult eyes were fixed with 4% paraformaldehyde in PBS for 20 min at room temperature. Tissues were permeabilized with 0.3% Triton X-100 (Sigma, T8787)-PBS and blocked with 5% normal goat serum (Gibco, 16210072) in 0.1% Triton-PBS. Samples were then stained with Hoechst (Invitrogen, H1399) or phalloidin (Sigma, SI-P1951) and mounted in 90% glycerol in PBS. Fly images were acquired with a confocal laser scanning microscope (Olympus FV3000). For immunofluorescence analysis of mammalian cells, cells grown to subconfluence on coverslips were washed with PBS and fixed with either 4% paraformaldehyde for 15 min or 100% methanol for 10 min. Cells were permeabilized with 0.2% Triton X-100, blocked with 2% BSA (UniRegion Bio-Tech, UR-BSA001), and incubated with primary antibody in PBS at 4°C overnight. After two washes with PBST (PBS with 0.05% Tween-20), secondary antibodies were added and incubated at room temperature for at least 1 h. After two more washes with PBST, cells were stained with DAPI and mounted with Fluoromount-G (Invitrogen, 00495952). Images were acquired with a confocal laser scanning microscope (Zeiss LSM510).

### In vitro membrane fusion assay

The in vitro membrane fusion assays were performed as previously described [55,56]. Briefly, cells transfected with either GFP-ATG16L1 or RFP-ATG16L1 were harvested in the homogenization buffer (250 mM sucrose [Merck, 57–50-1] and 3 mM imidazole, pH 7.4, protease inhibitor cocktail, 0.2 mM PMSF) and disrupted with glass beads. The cell lysates were then passed through a 22-guage syringe needle 20 times and centrifuged at 1200xg for 5 min at 4°C. The postnuclear supernatants which contained either the GFP-ATG16L1-positive vesicles or the RFP-ATG16L1-positive vesicles were mixed in the presence or absence of an ATP regenerative system at 37°C for 1 h. The mixed samples were mounted on glass slides and images were acquired using a Zeiss LSM510 confocal microscope.

### Electron microscopy

Cells seeded on ACLAR film (EMS, 50425–10) were cultured in EBSS medium for 1.5 h, fixed with 2.5% glutaraldehyde in PBS for 30 min, followed by postfixation buffer (1% $OsO_4$ in PBS) for 1 h. Samples were dehydrated in a graded series of ethanol, embedded with Spurr's resin (EMS, 14300), and sectioned at a thickness of 90 nm with the Leica EM UC6 ultramicrotome. The ultrathin sections were stained with 1% uranyl acetate, 5% lead citrate and images were acquired by a FEI Tecnai G2-F20 S-TWIN field emission gun (FEG) transmission electron microscope.

### Mass spectrometry analysis

Control and sh*Ptpn9* N2a cells transfected with a plasmid encoding Flag-VTI1B were starved for 1 h, lysed and samples were immunoprecipitated with anti-Flag antibody, resolved by SDS-PAGE, and then subjected to SYPRO Ruby (Invitrogen, S12000) staining. The Flag-VTI1B band was excised, in-gel digested with Lys-C (Wako, 125–05061)/trypsin (Promega, V5111), and subjected to liquid chromatography-tandem mass spectrometry (LC-MS/MS) analysis. The nanoLC-nanoESI-MS /MS analysis was performed using a nanoAcquity system (Waters, Milford, MA, USA) connected to the Orbitrap Elite hybrid mass spectrometer (Thermo Electron, Bremen, Germany) equipped with a PicoView nanospray interface (New Objective, Woburn, MA, USA). The data obtained from LC-MS/MS acquisition were processed by Proteome Discoverer (v2.4.1.15; Thermo Scientific) and searched against Swiss-Prot protein sequence database with the Mascot Daemon server (v.2.7.0; Matrix Science). For label-free quantification, precursor ions areas were extracted using Minora Feature Detector node in Proteome Discoverer 2.4 with a 10 ppm mass precision and 2 min retention time shift (align the LC/MS peaks mapping to the isotope pattern and retention time). The ratios for each peptide were normalized by the total identified peptides, and the ratios were used for protein-level quantification. Phosphorylation sites and peptide sequence assignments contained in MASCOT search results were validated by manual confirmation from raw MS/MS data.

### Statistical analysis

All data points were presented as mean ± SEM. Statistical analysis was performed by Student's t test for comparisons between two groups. Comparisons between more than two groups were performed using ANOVA and Tukey's multiple comparison tests in GraphPad Prism 7.0. Differences were considered significant if p values were less than 0.05 (*), 0.01 (**), 0.001 (***).

## Acknowledgments

We thank Drs Ruey-Hwa Chen, Zvulun Elazar, Yi-Shuian Huang, Nicholas Ktistakis, Ichiro Nakagawa, Jim Norman, Horng-Dar Wang, and Wei Yuan Yang, the Bloomington Stock Center, Vienna *Drosophila* RNAi Center, and Fly Core Taiwan for reagents and fly stocks; the National RNAi Core Facility for shRNAs; the Life Sciences Electron Microscope Lab (Academia Sinica) for electron microscopy assistance; Academia Sinica Common Mass Spectrometry Facilities for Proteomics and Protein Modification Analysis, which is supported by the Academia Sinica Core Facility and Innovative Instrument Project (AS-CFII-108-107), for mass spectrometry analysis. We thank Dr Chi-Kuang Yao for helpful discussions on the manuscript and James Steed for English editing. We are grateful to members of the Chen laboratory for helpful discussions during the course of this work.

## Disclosure statement

The authors declare no conflict of interest.

## Funding

This work was supported by the Ministry of Science and Technology, Taiwan (MOST108-2311-B-001-014-MY3) and by Academia Sinica (101CDA-L04).

## ORCID

Guang-Chao Chen http://orcid.org/0000-0002-4980-4718

## References

[1] Mizushima N. Autophagy: process and function. Genes Dev. 2007 Nov 15;21(22):2861–2873. PubMed PMID: 18006683; eng.
[2] Grasso D, Renna FJ, Vaccaro MI. Initial steps in mammalian autophagosome biogenesis. Front Cell Dev Biol. 2018;6:146. PubMed PMID: 30406104; PubMed Central PMCID: PMC6206277.
[3] Graef M, Friedman JR, Graham C, et al. ER exit sites are physical and functional core autophagosome biogenesis components. Mol Biol Cell. 2013 Sep;24(18):2918–2931. PubMed PMID: 23904270; PubMed Central PMCID: PMC3771953.
[4] Ge L, Melville D, Zhang M, et al. The ER-Golgi intermediate compartment is a key membrane source for the LC3 lipidation step of autophagosome biogenesis. eLife. 2013 Aug 6;2:e00947. PubMed PMID: 23930225; PubMed Central PMCID: PMC3736544.
[5] Guo Y, Chang C, Huang R, et al. AP1 is essential for generation of autophagosomes from the trans-Golgi network. J Cell Sci. 2012 Apr 1;125(Pt 7):1706–1715. PubMed PMID: 22328508.
[6] Hailey DW, Rambold AS, Satpute-Krishnan P, et al. Mitochondria supply membranes for autophagosome biogenesis during starvation. Cell. 2010 May 14;141(4):656–667. PubMed PMID: 20478256; PubMed Central PMCID: PMC3059894. eng.
[7] Hamasaki M, Furuta N, Matsuda A, et al. Autophagosomes form at ER-mitochondria contact sites. Nature. 2013 Mar 21;495 (7441):389–393. PubMed PMID: 23455425.
[8] Ravikumar B, Moreau K, Jahreiss L, et al. Plasma membrane contributes to the formation of pre-autophagosomal structures. Nat Cell Biol. 2010 Aug;12(8):747–757. PubMed PMID: 20639872; PubMed Central PMCID: PMC2923063. eng.
[9] Puri C, Vicinanza M, Rubinsztein DC. Phagophores evolve from recycling endosomes. Autophagy. 2018;14(8):1475–1477. PubMed PMID: 29940791; PubMed Central PMCID: PMCPMC6103687.
[10] Moreau K, Ravikumar B, Renna M, et al. Autophagosome precursor maturation requires homotypic fusion. Cell. 2011 Jul 22;146(2):303–317. PubMed PMID: 21784250; PubMed Central PMCID: PMCPMC3171170.
[11] Imai K, Hao F, Fujita N, et al. Atg9A trafficking through the recycling endosomes is required for autophagosome formation. J Cell Sci. 2016 Oct 15;129(20):3781–3791. PubMed PMID: 27587839.
[12] Xie Y, Kang R, Sun X, et al. Posttranslational modification of autophagy-related proteins in macroautophagy. Autophagy. 2015;11(1):28–45. PubMed PMID: 25484070; PubMed Central PMCID: PMCPMC4502723.
[13] Hunter T. Tyrosine phosphorylation: thirty years and counting. Curr Opin Cell Biol. 2009;21:140–146.
[14] Wei Y, Zou Z, Becker N, et al. EGFR-mediated Beclin 1 phosphorylation in autophagy suppression, tumor progression, and tumor chemoresistance. Cell. 2013 Sep 12;154(6):1269–1284. PubMed PMID: 24034250; PubMed Central PMCID: PMCPMC3917713.
[15] Martin KR, Xu Y, Looyenga BD, et al. Identification of PTPsigma as an autophagic phosphatase. J Cell Sci. 2011 Mar 1;124(Pt 5):812–819. PubMed PMID: 21303930; PubMed Central PMCID: PMCPMC3039021.
[16] Hatzihristidis T, Desai N, Hutchins AP, et al. A Drosophila-centric view of protein tyrosine phosphatases. FEBS Lett. 2015 Apr 13;589 (9):951–966. PubMed PMID: 25771859.

[17] Huynh H, Wang X, Li W, et al. Homotypic secretory vesicle fusion induced by the protein tyrosine phosphatase MEG2 depends on polyphosphoinositides in T cells. J Immunol. 2003 Dec 15;171(12):6661–6671. PubMed PMID: 14662869.
[18] Huynh H, Bottini N, Williams S, et al. Control of vesicle fusion by a tyrosine phosphatase. Nat Cell Biol. 2004 Sep;6(9):831–839. PubMed PMID: 15322554. DOI:10.1038/ncb1164
[19] Wang X, Huynh H, Gjorloff-Wingren A, et al. Enlargement of secretory vesicles by protein tyrosine phosphatase PTP-MEG2 in rat basophilic leukemia mast cells and Jurkat T cells. J Immunol. 2002 May 1;168(9):4612–4619. PubMed PMID: 11971009.
[20] Wang Y, Vachon E, Zhang J, et al. Tyrosine phosphatase MEG2 modulates murine development and platelet and lymphocyte activation through secretory vesicle function. J Exp Med. 2005 Dec 5;202(11):1587–1597. PubMed PMID: 16330817; PubMed Central PMCID: PMCPMC2213338.
[21] Yuan T, Wang Y, Zhao ZJ, et al. Protein-tyrosine phosphatase PTPN9 negatively regulates ErbB2 and epidermal growth factor receptor signaling in breast cancer cells. J Biol Chem. 2010 May 14;285(20):14861–14870. PubMed PMID: 20335174; PubMed Central PMCID: PMCPMC2865303.
[22] Cho CY, Koo SH, Wang Y, et al. Identification of the tyrosine phosphatase PTP-MEG2 as an antagonist of hepatic insulin signaling. Cell Metab. 2006 May;3(5):367–378. PubMed PMID: 16679294. DOI:10.1016/j.cmet.2006.03.006
[23] Wang Y, Li L, Hou C, et al. SNARE-mediated membrane fusion in autophagy. Semin Cell Dev Biol. 2016 Dec;60:97–104. PubMed PMID: 27422330; PubMed Central PMCID: PMCPMC5161566.
[24] Rusten TE, Lindmo K, Juhasz G, et al. Programmed autophagy in the Drosophila fat body is induced by ecdysone through regulation of the PI3K pathway. Dev Cell. 2004 Aug;7(2):179–192. PubMed PMID: 15296715. DOI:10.1016/j.devcel.2004.07.005
[25] Vietri M, Radulovic M, Stenmark H. The many functions of ESCRTs. Nat Rev Mol Cell Biol. 2019 Nov 8. PubMed PMID: 31705132. DOI:10.1038/s41580-019-0177-4
[26] Nezis IP, Shravage BV, Sagona AP, et al. Autophagic degradation of dBruce controls DNA fragmentation in nurse cells during late Drosophila melanogaster oogenesis. J Cell Biol. 2010 Aug 23;190(4):523–531. PubMed PMID: 20713604; PubMed Central PMCID: PMCPMC2928014.
[27] Lamb CA, Yoshimori T, Tooze SA. The autophagosome: origins unknown, biogenesis complex. Nat Rev Mol Cell Biol. 2013 Dec;14(12):759–774. PubMed PMID: 24201109.
[28] Axe EL, Walker SA, Manifava M, et al. Autophagosome formation from membrane compartments enriched in phosphatidylinositol 3-phosphate and dynamically connected to the endoplasmic reticulum. J Cell Biol. 2008 Aug 25;182(4):685–701. PubMed PMID: 18725538.
[29] Dooley HC, Razi M, Polson HE, et al. WIPI2 links LC3 conjugation with PI3P, autophagosome formation, and pathogen clearance by recruiting Atg12-5-16L1. Mol Cell. 2014 Jul 17;55(2):238–252. PubMed PMID: 24954904; PubMed Central PMCID: PMCPMC4104028.
[30] Itakura E, Kishi-Itakura C, Mizushima N. The hairpin-type tail-anchored SNARE syntaxin 17 targets to autophagosomes for fusion with endosomes/lysosomes. Cell. 2012 Dec 7;151(6):1256–1269. PubMed PMID: 23217709.
[31] Li J, Chen Z, Stang MT, et al. Transiently expressed ATG16L1 inhibits autophagosome biogenesis and aberrantly targets RAB11-positive recycling endosomes. Autophagy. 2017 Feb;13(2):345–358. PubMed PMID: 27875067; PubMed Central PMCID: PMCPMC5724932.
[32] Puri C, Renna M, Bento CF, et al. Diverse autophagosome membrane sources coalesce in recycling endosomes. Cell. 2013 Sep 12;154(6):1285–1299. PubMed PMID: 24034251; PubMed Central PMCID: PMCPMC3791395.
[33] Flint AJ, Tiganis T, Barford D, et al. Development of "substrate-trapping" mutants to identify physiological substrates of protein tyrosine phosphatases. Proc Natl Acad Sci U S A. 1997 Mar 4;94(5):1680–1685. PubMed PMID: 9050838; PubMed Central PMCID: PMCPMC19976.
[34] Hao Q, Samten B, Ji HL, et al. Tyrosine phosphatase PTP-MEG2 negatively regulates vascular endothelial growth factor receptor signaling and function in endothelial cells. Am J Physiol Cell Physiol. 2012 Sep 1;303(5):C548–53. PubMed PMID: 22763125; PubMed Central PMCID: PMCPMC3468344.
[35] Burgo A, Casano AM, Kuster A, et al. Increased activity of the vesicular soluble N-ethylmaleimide-sensitive factor attachment protein receptor TI-VAMP/VAMP7 by tyrosine phosphorylation in the Longin domain. J Biol Chem. 2013 Apr 26;288(17):11960–11972. PubMed PMID: 23471971; PubMed Central PMCID: PMCPMC3636883.
[36] Emperador-Melero J, Toonen RF, Verhage M. Vti proteins: beyond endolysosomal trafficking. Neuroscience. 2019 Nov 10;420:32–40. PubMed PMID: 30471354.
[37] Furuta N, Fujita N, Noda T, et al. Combinational soluble N-ethylmaleimide-sensitive factor attachment protein receptor proteins VAMP8 and Vti1b mediate fusion of antimicrobial and canonical autophagosomes with lysosomes. Mol Biol Cell. 2010 Mar 15;21(6):1001–1010. PubMed PMID: 20089838; PubMed Central PMCID: PMCPMC2836953.
[38] Kimura S, Noda T, Yoshimori T. Dissection of the autophagosome maturation process by a novel reporter protein, tandem fluorescent-tagged LC3. Autophagy. 2007 Sep-Oct;3(5):452–460. PubMed PMID: 17534139.
[39] Abada A, Levin-Zaidman S, Porat Z, et al. SNARE priming is essential for maturation of autophagosomes but not for their formation. Proc Natl Acad Sci U S A. 2017 Nov 28;114(48):12749–12754. PubMed PMID: 29138318; PubMed Central PMCID: PMCPMC5715740.
[40] Menzies FM, Fleming A, Caricasole A, et al. Autophagy and neurodegeneration: pathogenic Mechanisms and therapeutic opportunities. Neuron. 2017 Mar 8;93(5):1015–1034. PubMed PMID: 28279350.
[41] Fujikake N, Shin M, Shimizu S. Association between autophagy and neurodegenerative diseases. Front Neurosci. 2018;12:255. PubMed PMID: 29872373; PubMed Central PMCID: PMCPMC5972210.
[42] Sang TK, Li C, Liu W, et al. Inactivation of Drosophila Apaf-1 related killer suppresses formation of polyglutamine aggregates and blocks polyglutamine pathogenesis. Hum Mol Genet. 2005 Feb 1;14(3):357–372. PubMed PMID: 15590702.
[43] Charlton-Perkins M, Cook TA. Building a fly eye: terminal differentiation events of the retina, corneal lens, and pigmented epithelia. Curr Top Dev Biol. 2010;93:129–173. PubMed PMID: 20959165; PubMed Central PMCID: PMCPMC5534335.
[44] Zhao YG, Zhang H. Autophagosome maturation: an epic journey from the ER to lysosomes. J Cell Biol. 2019 Mar 4;218(3):757–770. PubMed PMID: 30578282; PubMed Central PMCID: PMCPMC6400552.
[45] Guo B, Liang Q, Li L, et al. O-GlcNAc-modification of SNAP-29 regulates autophagosome maturation. Nat Cell Biol. 2014 Dec;16(12):1215–1226. PubMed PMID: 25419848.
[46] Malmersjo S, Di Palma S, Diao J, et al. Phosphorylation of residues inside the SNARE complex suppresses secretory vesicle fusion. Embo J. 2016 Aug 15;35(16):1810–1821. PubMed PMID: 27402227; PubMed Central PMCID: PMCPMC5010044.
[47] Laidlaw KME, Livingstone R, Al-Tobi M, et al. SNARE phosphorylation: a control mechanism for insulin-stimulated glucose transport and other regulated exocytic events. Biochem Soc Trans. 2017 Dec 15;45(6):1271–1277. PubMed PMID: 29101310.
[48] Kumar S, Gu Y, Abudu YP, et al. Phosphorylation of syntaxin 17 by TBK1 controls autophagy initiation. Dev Cell. 2019 Apr 8;49(1):130–144e6. PubMed PMID: 30827897.
[49] Nozawa T, Minowa-Nozawa A, Aikawa C, et al. The STX6-VTI1B-VAMP3 complex facilitates xenophagy by regulating the fusion between recycling endosomes and autophagosomes. Autophagy. 2017 Jan 2;13(1):57–69. PubMed PMID: 27791468; PubMed Central PMCID: PMCPMC5240839.

[50] Pohl C, Dikic I. Cellular quality control by the ubiquitin-proteasome system and autophagy. Science. 2019 Nov 15;366(6467):818–822. PubMed PMID: 31727826.

[51] Krench M, Littleton JT. Neurotoxicity pathways in Drosophila models of the polyglutamine disorders. Curr Top Dev Biol. 2017;121:201–223. PubMed PMID: 28057300.

[52] Chen DY, Li MY, Wu SY, et al. The Bro1-domain-containing protein Myopic/HDPTP coordinates with Rab4 to regulate cell adhesion and migration. J Cell Sci. 2012 Oct 15;125(Pt 20):4841–4852. PubMed PMID: 22825871.

[53] Chen SF, Kang ML, Chen YC, et al. Autophagy-related gene 7 is downstream of heat shock protein 27 in the regulation of eye morphology, polyglutamine toxicity, and lifespan in Drosophila. J Biomed Sci. 2012 May 23;19:52. PubMed PMID: 22621211; PubMed Central PMCID: PMCPMC3483682.

[54] Tang HW, Liao HM, Peng WH, et al. Atg9 interacts with dTRAF2/TRAF6 to regulate oxidative stress-induced JNK activation and autophagy induction. Dev Cell. 2013 Dec 9;27(5):489–503. PubMed PMID: 24268699.

[55] Barysch SV, Jahn R, Rizzoli SO. A fluorescence-based in vitro assay for investigating early endosome dynamics. Nat Protoc. 2010 Jun;5(6):1127–1137. PubMed PMID: 20539288.

[56] Moreau K, Puri C, Rubinsztein DC. Methods to analyze SNARE-dependent vesicular fusion events that regulate autophagosome biogenesis. Methods. 2015 Mar;75:19–24. PubMed PMID: 25461811; PubMed Central PMCID: PMC4358838.